ChemComm

COMMUNICATION

View Article Online
View Journal | View Issue

Cite this: *Chem. Commun.*, 2019, **55**, 2988

Received 23rd November 2018,
Accepted 29th January 2019

DOI: 10.1039/c8cc09321k

rsc.li/chemcomm

Non-empirical calculation of X-ray magnetic circular dichroism in lanthanide compounds†

Harry Ramanantoanina, * Michał Studniarek, Niéli Daffé and Jan Dreiser *

Affordable calculations of X-ray magnetic circular dichroism and X-ray linear dichroism spectra of lanthanide ions purely based on structural input are difficult to achieve. Here we report on the successful application of ligand-field density-functional theory to obtain an exquisite reproduction of experimental spectra. As a testbed we use $TbPc_2$ single-molecule magnets on a flat substrate.

X-ray magnetic circular dichroism (XMCD) and X-ray linear dichroism (XLD) at the $L_{2,3}$ edges of transition metals and at the $M_{4,5}$ edges of lanthanides are increasingly employed for the study of an enormous variety of magnetic materials.[1] XMCD probes the spin and orbital magnetic moments residing in the open d or f shell, respectively, by performing X-ray absorption spectroscopy (XAS) with the two circular polarizations of the X-rays.[2] Its element specificity and ultrahigh sensitivity, owing to the very large absorption cross sections in the soft X-ray range, allow one to obtain insights, which are not possible or difficult to achieve with other techniques.

Despite the success of the XMCD method it is still a challenge to perform reliable calculations of the obtained X-ray absorption and XMCD/XLD spectra based on purely structural input. The most widespread approach, due to its simplicity and efficiency, is ligand-field multiplet theory (LFMT),[3–7] which is extremely successful in reproducing the spectral shapes of lanthanide $M_{4,5}$ spectra. However, these calculations heavily rely on empirical parameterization of the ligand-field Hamiltonian as well as on empirical adjustments of the Slater–Condon integrals and spin–orbit coupling constants with multiplication factors. The parameterization of the ligand-field potential is a problem in particular, since in the absence of any symmetry up to 15 + 28 independent parameters would be needed for a full description.[8] While one-electron approaches using density-functional theory (DFT) calculations are interesting because of the strengths in structural modeling, these calculations are not designed to take into account the core-hole and valence electron interactions that are created during the X-ray absorption process.[9] Hybrid approaches, in which ligand-field parameters of LFMT are obtained by electronic structure calculations, have been demonstrated for 3d transition metals XAS.[7,10,11] The feasibility in the case of 4f lanthanides and 5f actinides application is possible but much effort is needed to establish a fully non-empirical model.[12,13]

Here, we demonstrate that ligand-field density-functional theory (LFDFT)[14–17] is able to reproduce in very detail the XMCD spectra as well as the corresponding XLD. As an example we employ the case of $TbPc_2$ [bis(phthalo-cyaninato)terbium(III)] single-molecule magnets[18] (Fig. 1a) adsorbed as a submonolayer on a flat and weakly interacting oxide surface.[19] The method is particularly well suitable to treat the 4f shell magnetism because of the inner-shell nature and because of the rather low hybridization of 4f electrons, as compared to 3d transition metals, with the environment of the atom under consideration.

Details about the application of LFDFT to calculate unpolarized XAS can be found in ref. 13. Here we describe the extension of the method to obtain polarized X-ray spectra. Using DFT we set up an active subspace of Kohn–Sham orbitals that forms the basis of the fivefold 3d and sevenfold 4f orbitals of the trivalent lanthanide ions with the $3d^{10}4f^{n}$ ground state and the $3d^{9}4f^{n+1}$ excited state configurations, respectively. This active subspace is defined with a fractional occupation of electrons, where the smearing of the electrons onto the manifolds of the 3d and 4f orbitals allows obtaining the electronic density that belongs to the totally symmetric representation under which the effective ligand-field Hamiltonian (eqn (1)) is operated.[12–17]

$$H_{\mathrm{eff}} = H_0 + H_{\mathrm{ER}} + H_{\mathrm{SO}} + H_{\mathrm{LF}} + H_{\mathrm{ZE}}, \quad (1)$$

The interaction matrices for the configuration average energy correction (H_0), electrostatic inter-electron repulsion (H_{ER}),

Paul Scherrer Institute, CH-5232, Villigen PSI, Switzerland.
E-mail: harry.ra@hotmail.com, jan.dreiser@psi.ch

† Electronic supplementary information (ESI) available: Computational details; optimized DFT geometrical structure of $TbPc_2$ and comparison with experimental structure; atomic cartesian coordinates; selected Kohn–Sham orbital energies and wavefunctions; calculated parameters and ligand-field matrix elements within the ground state and excited state configurations; calculated energy levels of the $^7F_6$ ground state atomic multiplet of Tb^{3+} in $TbPc_2$; selected energy levels of the excited state $3d^94f^9$ configuration of Tb^{3+} in $TbPc_2$; residual plots of the polarized X-ray spectra. See DOI: 10.1039/c8cc09321k

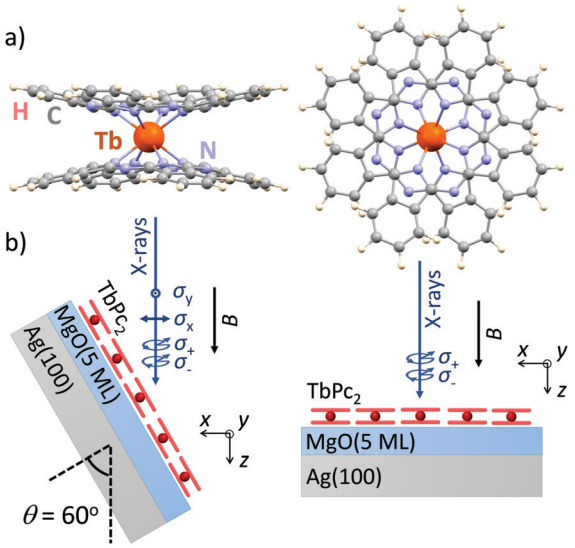

Fig. 1 (a) Molecular structure of $TbPc_2$ used as input for the calculations. View perpendicular to (left) and along (right) the main fourfold symmetry axis. (b) Experimental geometry used to acquire the X-ray spectra with normal (θ = 0°) and grazing (θ = 60°) X-ray incidence, with $\sigma_+(\sigma_-)$ denoting circular right (left) X-ray polarization, and $\sigma_y(\sigma_x)$ linear vertical (horizontal) polarization, respectively.

spin–orbit coupling (H_{SO}) and ligand-field splitting (H_{LF}) are constructed.[12–17] The input parameters include the energy gap (ΔE_{av}), Slater–Condon integrals (F^k(4f,4f), with k = 2, 4 and 6; F^k(3d,4f), with k = 2 and 4; and G^k(3d,4f), with k = 1, 3 and 5), spin–orbit coupling constants (ζ_{3d} and ζ_{4f}) and ligand-field potential (a matrix with 12 × 12 elements), where in total 155 parameter values are non-empirically extracted from the DFT calculation.[12–17] The eigendecomposition of the matrix elements of the effective Hamiltonian in eqn (1) yields the multiplet energies (E) and the multi-electronic eigenfunctions (ψ) that arise from the open-shell configurations $3d^{10}4f^n$ and $3d^94f^{n+1}$ of the trivalent lanthanide ions.

In the context of the magnetic dichroism experiment, *i.e.* in the presence of an external magnetic field (B), we add an extra term in eqn (1) that represents the electronic Zeeman interaction (H_{ZE}).[20] This term is defined as follows:

$$H_{ZE} = \mu_B(g_L\boldsymbol{L} + g_e\boldsymbol{S})\cdot\boldsymbol{B}, \quad (2)$$

where, $\mu_B = e\hbar/(2mc)$ is the Bohr magneton; $\boldsymbol{L}$ and $\boldsymbol{S}$ are the orbital angular momentum and spin operators; $g_L \approx 1$ and $g_e \approx 2$ are the electron orbital and spin g-factors, respectively.

We use the electric dipole approximation to model the X-ray absorption spectrum. The excitation energies and oscillator strengths of the intra-atomic $3d^{10}4f^n + h\nu \rightarrow 3d^94f^{n+1}$ electron transitions are defined as follows:

$$E_{ph} = \Delta E_{i,j} = E_j - E_i^{(0)}, \quad (3)$$

$$\boldsymbol{\mu}(E) \cong \frac{1}{Z}\sum_{j=1}^{N_f}\sum_{i=1}^{N_i}\exp\left(-\frac{E_i^{(0)}}{k_BT}\right)\left|\left\langle\psi_j|\boldsymbol{d}|\psi_i^{(0)}\right\rangle\right|^2\delta(E-\Delta E_{i,j}) \quad (4)$$

where, $(E^{(0)}, \psi^{(0)})$ are the multiplet energies and multi-electronic eigenfunctions that are calculated for the initial state $3d^{10}4f^n$ electron configuration of the trivalent lanthanide ions; (E, ψ) represents the multiplet energies and multi-electronic eigenfunctions that are calculated for the excited state $3d^94f^{n+1}$ electron configuration; and $\langle\psi_j|\boldsymbol{d}|\psi_i^{(0)}\rangle$ is the transition amplitude between the two states with the electric-dipole moment operator $\boldsymbol{d}$. The outer sums run over the number of states N_i and N_f of the initial $3d^{10}4f^n$ and final $3d^94f^{n+1}$ state configurations and Z is the partition function $Z = \sum_{k=1}^{N(3d^{10}4f^n)}\exp\left(-E_k^{(0)}/k_BT\right)$. The Boltzmann distribution in eqn (4) is taken over the manifold of the initial state configuration to account for finite temperature effects.

The electric dipole moment operator is split into three components that correspond to e_x, e_y and e_z polarizations with $\boldsymbol{e}$ the vector of the oscillating electric field. The z term gives the absorption for the electric vector parallel to the magnetic axis, and the sum of the x and y terms gives the intensity for the oscillating electric field perpendicular to the magnetic axis. The XLD is defined as the difference in absorption of linearly polarized light, XLD = $\mu_y - \mu_x$, induced by the 4f ligand-field splitting and the resulting different orbital occupation. On the other hand, the magnetic circular dichroism is defined as the difference in absorption with respect to the left circular (μ_-) and right circular (μ_+) light $e_\pm = (e_x \pm i\cdot e_y)/\sqrt{2}$. Hence, XMCD = [$\mu_+ - \mu_-$], and it is induced by the presence of a magnetic moment residing in the 4f shell.

In order to make the calculated absorption spectra comparable to the experimental ones, they are convoluted with a Lorentzian function. The full width at half maximum (FWHM) was 1.0 eV and for simplicity only a single line width function was applied in the whole energy range to take into account both the core-hole lifetime and instrumental broadenings.

The DFT calculations were performed by means of the Amsterdam density functional (ADF) program package.[21] Details about the computational procedure are given in the ESI,† Computational details section. We used the DFT relaxed structure of the isolated $TbPc_2$ molecule as input geometry corresponding to the molecular gas phase. The DFT equilibrium geometry is in good agreement with the experimental structure[22] (*cf.* ESI,† Fig. S1 and Table S1). The optimized Cartesian coordinates are given in the ESI,† Table S2. The calculated energy values of the Kohn–Sham orbitals of $TbPc_2$ in the −6.125 eV to −4.425 eV energy range are listed in the ESI,† Table S3 together with the parentage of $TbPc_2$ from Tb 3d and 4f atomic orbitals and the occupation scheme that was imposed in the DFT calculations. Seven Kohn–Sham Orbitals have nearly atomic-like Tb 4f character, with percentage characters larger than 90% (*cf.* ESI,† Table S3). These orbitals have been used as the active subspace that resolved the 4f ligand-field states of the Tb^{3+} ion. Based on this active subspace together with the Tb core 3d functions, the non-empirical parameters that are used as input of the effective ligand-field Hamiltonian in eqn (1) were obtained using the newly available LFDFT keyword in the ADF program package.[21] Their tabulated values are listed in the ESI† (Tables S4–S7) for both ground state ($3d^{10}4f^8$) and excited state ($3d^94f^9$) electron configurations of Tb^{3+} in the complex $TbPc_2$. Note that the DFT calculations suggest the presence of hybridization or covalency

of Tb 4f orbitals with ligand orbitals in the few percent range. The hybridization is expected to be slightly overestimated due to the self-interaction error in DFT.[23] However, it does not affect the LF Hamiltonian, because the ligand contribution to the wave function is neglected.[24]

In order to validate the accuracy of the calculations we compare the simulated XAS, XMCD, and XLD spectra to the ones experimentally recorded on *ca.* 0.7 monolayers of $TbPc_2$ molecules (Fig. 1a) deposited on a MgO thin film. We selected this system because the phthalocyanine–MgO hybridization is expected to be weak[25] resulting in X-ray spectra of close-to-isolated (gas-phase-like, but spatially ordered) molecules, and because it is well known that the $TbPc_2$ molecules are arranged in self-assembled islands with their planar ligands parallel to the surface plane.[19] The molecules were sublimed from a Knudsen cell held at a temperature of 673 K onto the three monolayer thick film of MgO grown epitaxially on a Ag(100) crystal which has been cleaned previously by repeated Ar^+ ion sputter annealing cycles.

The experimental spectra were recorded on samples prepared similar to ref. 19 at the X-Treme beamline of the Swiss Light Source.[26] The XAS measurements were performed in normal ($\theta = 0^\circ$) and grazing ($\theta = 60^\circ$) incidence of the X-rays. We fix the frame of reference such that the z axis is along the X-ray propagation direction and at normal incidence the xy plane lies in the molecular plane, that is, in the plane of the phthalocyanine ligands (see Fig. 1b). All measurements were performed in total electron yield mode, and the magnetic field was always parallel to the beam propagation direction. A polynomial background was subtracted from the spectra.

The calculated XAS and the corresponding XMCD along with the experimental spectra acquired on the submonolayer of $TbPc_2$ molecules at both normal and grazing geometry are presented in Fig. 2. Note that the calculated spectra are obtained by means of LFDFT calculations using the DFT functional following the generalized gradient approximation formulation (see also the ESI,† Computational details section) and the optimized structure of $TbPc_2$ is obtained with the same DFT functional (see also the ESI,† Table S2). The ESI,† Tables S8 and S9 list the multiplet energy levels and the ligand-field splitting of the Tb^{3+} ion in $TbPc_2$ within the atomic ground state ($3d^{10}4f^8$) and excited state ($3d^94f^9$) configurations as well as the oscillator strengths of the $3d^{10}4f^8$–$3d^94f^9$ electron transitions. The calculated spectra were normalized in order to have the same Tb M_5 areas in the sum of the helicities as the experimental ones. Furthermore, the calculated spectra were shifted in photon energy by −3.1 eV to find the best match with the experiment. The comparison reveals that the simulated X-ray spectra are in excellent agreement with the experimental ones. The calculated differences between the simulated and experimental spectra, *i.e.*, the residuals, are plotted in the ESI,† Fig. S2, indicating a larger splitting of the main features of the M_5 edge in the calculations as already visible in Fig. 2. This is most likely due to a slight overestimation of the Slater–Condon parameters by LFDFT. Note that the inter-electron repulsion and spin–orbit coupling that induce the separation between the Tb M_5 and M_4 edges are obtained without any empirical correction in the present work. The strength of the XMCD signal is proportional to the Tb 4f magnetic moment projected onto the beam propagation vector.[1] In this context the reduced XMCD amplitude at grazing incidence with respect to normal geometry is in line with the known strong out-of-plane easy-axis magnetic anisotropy of the $TbPc_2$ molecules. Note that the XMCD spectra shown in Fig. 2 imply an excellent reproduction of the $TbPc_2$ magnetic properties by our calculations.

The XLD reflects the angular distribution of the 4f holes, and it thus provides information on the molecular orientation on the surface. We acquired the experimental XLD at grazing incidence (see Fig. 1b) by recording the XAS spectra with linear vertical polarization e_y probing 4f orbitals in the surface plane and linear horizontal polarization e_x probing mostly out-of-plane 4f orbitals. The comparison of the calculated XLD spectra with the experimental ones is presented in Fig. 3. Both the shape and the amplitude of the calculated linearly polarized spectra excellently match the experimental data. The energy of the maximum of the Tb M_5 edge depends on the linear polarization, that is, 1233.6 eV for the e_x polarization and 1235.8 eV for e_y, which indicates a preferential orientation of the $TbPc_2$ molecules on the surface with the phthalocyanine ligand plane parallel to the surface, as shown

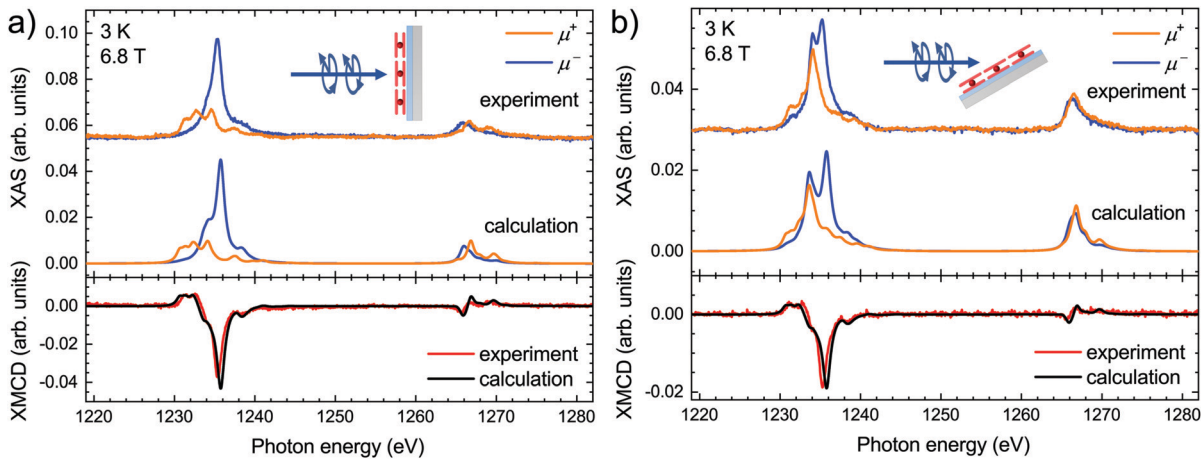

Fig. 2 Comparison of the calculated and experimentally acquired X-ray absorption spectra (top panels) and X-ray magnetic circular dichroism (bottom panels) at the Tb $M_{4,5}$ edges of $TbPc_2$ molecules at normal (a) and grazing (b) geometry.

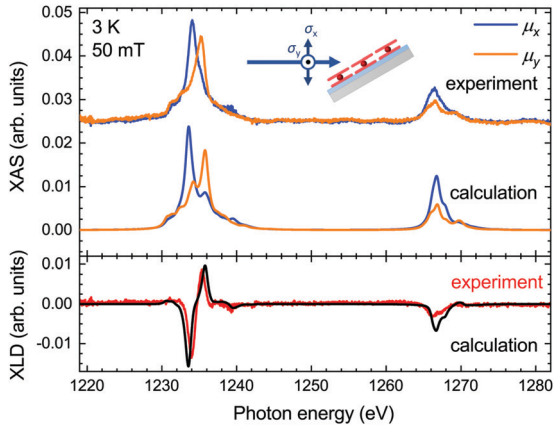

Fig. 3 Comparison of the calculated and experimentally acquired X-ray absorption spectra (top panel) and X-ray linear dichroism (bottom panel) at the Tb $M_{4,5}$ edges of $TbPc_2$ at grazing geometry.

by the STM studies[19] and in comparison with previous work.[27,28] The calculated spectra correctly reproduce these energetic positions of the main peak, albeit with a slightly larger splitting leading to weak satellite peaks at 1235.8 eV (1234.2 eV). The M_4 edge is slightly overestimated in the calculations, which might result from imperfections in the background subtraction and/or from a stronger line broadening at the M_4 edge, which was taken to be constant across the whole energy range for the sake of simplicity.

In conclusion, we have developed a DFT-based theoretical model for the calculation of the X-ray magnetic circular dichroism and X-ray linear dichroism spectra of lanthanide compounds. By using a ligand-field Hamiltonian in association with the DFT calculations, we are able to model the XMCD and XLD at the Tb $M_{4,5}$ edges of $TbPc_2$, taking into consideration all the quantum physical interactions involved in the X-ray absorption process such as the inter-electronic repulsion, spin–orbit coupling and ligand-field splitting of the atomic multiplet energies. The calculations are in excellent agreement with the experimental spectra, providing deep insight into the microscopic origin of dichroism in optical spectra and a good understanding of the mechanism of 3d core-electron excitation in Tb^{3+} ions. We have also shown that the computational cost is economic and the methodology does not require sophisticated DFT functionals or basis functions.

Thus LFDFT, which works for the whole lanthanide series, is an excellent and efficient non-empirical method able to model spectral profiles with relevance in the study of existing and future applications of trivalent lanthanide ions. The performance of the LFDFT method is promising for the calculation of XMCD spectra of lanthanide centers in low-symmetry geometries, which can occur, *e.g.*, in surface-adsorbed molecular magnets or atoms.

The authors thank Prof. Mario Ruben, Dr Svetlana Klyatskaya and Dr Yanhua Lan for providing the $TbPc_2$ molecules. This project was supported by funding from the European Union's Horizon 2020 research and innovation programme under the Marie Skłodowska-Curie grant agreement no. 701647. Furthermore, the authors acknowledge funding by Swissnuclear and by the Swiss National Science Foundation (grant no. 200021_165774/1).

Conflicts of interest

There are no conflicts to declare.

Notes and references

1 G. van der Laan and A. I. Figueroa, *Coord. Chem. Rev.*, 2014, **277–278**, 95–129.
2 J. Stöhr and H. C. Siegmann, *Magnetism: From Fundamentals to Nanoscale Dynamics*, Springer-Verlag, Berlin Heidelberg, 2006.
3 B. T. Thole, G. van der Laan and G. A. Sawatzky, *Phys. Rev. Lett.*, 1985, **55**, 2086–2088.
4 J. B. Goedkoop, B. T. Thole, G. van der Laan, G. A. Sawatzky, F. M. F. de Groot and J. C. Fuggle, *Phys. Rev. B: Condens. Matter Mater. Phys.*, 1988, **37**, 2086–2093.
5 F. de Groot, *Coord. Chem. Rev.*, 2005, **249**, 31–63.
6 A. Uldry, F. Vernay and B. Delley, *Phys. Rev. B: Condens. Matter Mater. Phys.*, 2012, **85**, 125133.
7 M. W. Haverkort, M. Zwierzycki and O. K. Andersen, *Phys. Rev. B: Condens. Matter Mater. Phys.*, 2012, **85**, 165113.
8 H. Ramanantoanina, W. Urland, F. Cimpoesu and C. Daul, *Phys. Chem. Chem. Phys.*, 2014, **16**, 12282–12290.
9 M. Roemelt, D. Maganas, S. DeBeer and F. Neese, *J. Chem. Phys.*, 2013, **138**, 204101.
10 H. Ikeno, T. Mizoguchi and I. Tanaka, *Phys. Rev. B: Condens. Matter Mater. Phys.*, 2011, **83**, 155107.
11 H. Ramanantoanina and C. Daul, *Phys. Chem. Chem. Phys.*, 2017, **19**, 20919–20929.
12 H. Ramanantoanina, *Phys. Chem. Chem. Phys.*, 2017, **19**, 32481–32491.
13 H. Ramanantoanina, *J. Chem. Phys.*, 2018, **149**, 054104.
14 M. Atanasov, C. A. Daul and C. Rauzy, in *Optical Spectra and Chemical Bonding in Inorganic Compounds: Special Volume dedicated to Professor Jørgensen I*, ed. D. M. P. Mingos and T. Schönherr, Springer Berlin Heidelberg, Berlin, Heidelberg, 2004, pp. 97–125.
15 M. Atanasov, C. Rauzy, P. Baettig and C. Daul, *Int. J. Quantum Chem.*, 2005, **102**, 119–131.
16 H. Ramanantoanina, W. Urland, F. Cimpoesu and C. Daul, *Phys. Chem. Chem. Phys.*, 2013, **15**, 13902–13910.
17 H. Ramanantoanina, M. Sahnoun, A. Barbiero, M. Ferbinteanu and F. Cimpoesu, *Phys. Chem. Chem. Phys.*, 2015, **17**, 18547–18557.
18 N. Ishikawa, M. Sugita, T. Ishikawa, S. Koshihara and Y. Kaizu, *J. Am. Chem. Soc.*, 2003, **125**, 8694–8695.
19 C. Wäckerlin, F. Donati, A. Singha, R. Baltic, S. Rusponi, K. Diller, F. Patthey, M. Pivetta, Y. Lan, S. Klyatskaya, M. Ruben, H. Brune and J. Dreiser, *Adv. Mater.*, 2016, **28**, 5195–5199.
20 A. Abragam and B. Bleaney, *Electron Paramagnetic Resonance of Transition Ions*, Oxford Classic Texts in the Physical Sciences, 1970.
21 E. J. Baerends, *et al.*, *ADF2017*, 2017, available at http://www.scm.com.
22 K. Katoh, Y. Yoshida, M. Yamashita, H. Miyasaka, B. K. Breedlove, T. Kajiwara, S. Takaishi, N. Ishikawa, H. Isshiki, Y. F. Zhang, T. Komeda, M. Yamagishi and J. Takeya, *J. Am. Chem. Soc.*, 2009, **131**, 9967–9976.
23 I. Ciofini, C. Adamo and H. Chermette, *Chem. Phys.*, 2005, **309**, 67–76.
24 B. N. Figgis and M. A. Hitchman, *Ligand field theory and its applications*, Wiley-VCH, 2000.
25 M. Glaser, H. Peisert, H. Adler, M. Polek, J. Uihlein, P. Nagel, M. Merz, S. Schuppler and T. Chassé, *J. Phys. Chem. C*, 2015, **119**, 27569–27579.
26 C. Piamonteze, U. Flechsig, S. Rusponi, J. Dreiser, J. Heidler, M. Schmidt, R. Wetter, M. Calvi, T. Schmidt, H. Pruchova, J. Krempasky, C. Quitmann, H. Brune and F. Nolting, *J. Synchrotron Radiat.*, 2012, **19**, 661–674.
27 S. Stepanow, J. Honolka, P. Gambardella, L. Vitali, N. Abdurakhmanova, T.-C. Tseng, S. Rauschenbach, S. L. Tait, V. Sessi, S. Klyatskaya, M. Ruben and K. Kern, *J. Am. Chem. Soc.*, 2010, **132**, 11900–11901.
28 L. Margheriti, D. Chiappe, M. Mannini, P. Car, P. Sainctavit, M.-A. Arrio, F. B. de Mongeot, J. C. Cezar, F. M. Piras, A. Magnani, E. Otero, A. Caneschi and R. Sessoli, *Adv. Mater.*, 2010, **22**, 5488–5493.